Basal Cell Carcinomas in Mice Overexpressing Sonic Hedgehog

Anthony E. Oro, Kay M. Higgins, Zhilan Hu, Jeannette M. Bonifas, Ervin H. Epstein Jr.,* Matthew P. Scott*

Mutations in the tumor suppressor gene *PATCHED* (*PTC*) are found in human patients with the basal cell nevus syndrome, a disease causing developmental defects and tumors, including basal cell carcinomas. Gene regulatory relationships defined in the fruit fly *Drosophila* suggest that overproduction of Sonic hedgehog (SHH), the ligand for PTC, will mimic loss of *ptc* function. It is shown here that transgenic mice overexpressing SHH in the skin develop many features of basal cell nevus syndrome, demonstrating that SHH is sufficient to induce basal cell carcinomas in mice. These data suggest that *SHH* may have a role in human tumorigenesis.

A large body of evidence supports the idea that multiple genetic events are required to transform normal epithelium into benign growths and then into metastatic tumors (*1*). Some types of tumors rarely show complete progression: For example, basal cell carcinomas (BCCs) of the skin—the most common tumors in Caucasians, with about 750,000 new cases annually in the United States—are generally only locally invasive (*2*). The lack of a mouse model of BCCs and the difficulty in culturing human BCCs has slowed progress in understanding the mechanisms underlying BCC biology.

Basal cell nevus syndrome (BCNS) is an autosomal dominant disease characterized by developmental defects and a predisposition to certain tumors (*3*). The most common morphologic abnormalities are skeletal defects such as polydactyly, jaw and rib defects, and spina bifida; the most common tumors are BCCs, medulloblastomas, and meningiomas. The defective gene is *ptc* (*4*), a gene on chromosome 9q, first identified in *Drosophila* as a regulator of embryonic pattern formation. Numerous sporadic BCCs also have 9q loss and *ptc* mutations, suggesting that many BCCs unrelated to BCNS arise from somatic damage to both copies of *ptc* (*4*, *5*).

The *ptc* gene encodes a transmembrane receptor that represses transcription of genes encoding transforming growth factor–β and Wnt class signaling proteins and *ptc* itself (6). One vertebrate PTC ligand is the secreted protein SHH, which binds to PTC in cultured cells and frog oocytes. The fly homolog of SHH, Hedgehog (HH), is believed to inactivate PTC function, suggesting that HH proteins induce target gene transcription by inactivating their receptor's function.

The COOH-terminal part of SHH is an autoprotease and cholesterol transferase that cleaves the SHH precursor into two fragments and adds a cholesterol moiety to the NH_2-terminal fragment (6). The latter fragment is sufficient for all known signaling events and contains a zinc hydrolase-like domain that may act as a peptidase (*6*, *7*). Thus, in addition to binding to PTC, SHH may cleave an unknown target molecule, although no catalytic activity has yet been detected. In *Drosophila*, *ptc* represses its target genes except where *ptc* function is inactivated by *Hh*, and this relationship appears to be conserved in vertebrates. Excess *Hh* function has an effect similar to loss of *ptc* function (*8*). This genetic relationship means that overexpression of *Shh* in mouse skin might mimic the loss of *ptc* function seen in human BCCs.

In normal mice, *Shh* and *ptc* RNA accumulate in follicular but not interfollicular skin. Initial expression of *Shh* and *ptc* in skin occurs in Hardy stage 1 hair follicles. In 14.5-day postcoital (dpc) skin, *Shh* RNA accumulates at regularly spaced intervals in the ectoderm. Each spot of *Shh* signal overlies the mesenchymal condensation of a presumptive follicle (*9*) (Fig. 1A). High levels of *ptc* RNA accumulate in each underlying mesenchymal condensation and at slightly lower levels in the *Shh*-expressing ectodermal cells (Fig. 1B), presumably because of induction of *ptc* transcription by SHH (*10*).

To examine in vivo the effect of excess SHH signaling, we generated transgenic mice that overexpress SHH specifically in the skin. We fused *Shh* to the keratin 14 (K14) promoter (Fig. 1I) (*11*), which drives expression as early as 9.5 dpc in the ectoderm and at later stages in both the follicular and interfollicular epithelium (*12*). In total, 26 transgenic mice derived from pronuclear injection were examined as embryos or neonates; lines could not be established because of perinatal lethality. In transgenic embryos, high levels of *Shh* RNA and *ptc* RNA accumulated in the basal layer of the epidermis, both in the follicular and the interfollicular epithelium (Fig. 1, C and D). The heightened *ptc* expression confirmed that functional SHH was present and capable of inducing the *ptc* target gene in epidermal cells. The *ptc* transcripts were also present in the mesenchyme underlying the ectoderm of transgenics, presumably resulting from movement of SHH into these cells.

The K14-*Shh* transgenic mice exhibited skeletal and skin abnormalities reminiscent of those seen in BCNS. The most frequent abnormality was polydactyly of both the fore- and hind limbs, some of which had eight digits (Fig. 1E). Each digit looked similar to the normal central digits, as in the chick *talpid*^{3} mutant (*13*). Distal phalanges were often missing, giving rise to a shortened but wider limb. Distal cartilage bifurcations, ectopic sites of cartilage formation between the digits, and a distal rim of persistent ossification were apparent. Spina bifida, a failure to close the neural tube, was also frequently observed in the transgenics. This defect always affected the caudal portion of the spine and, in severe mutants, extended to the thoracic spine. Skeletal preparations revealed that spinal processes that normally enclose the spinal cord failed to form dorsally (Fig. 1F) (*14*). These effects on skeletal development suggest that SHH penetrates internal tissues, as does the mesenchymal ectopic *ptc* expression.

The K14-*Shh* transgenic mice had multiple BCC-like epidermal proliferations throughout their skin surface after only the first few days of skin development. Dead perinatal embryos invariably had erosions that destroyed much of the skin surface. The skin lacked normal folds and was translucent and friable (Fig. 1H). Skin histology revealed massive proliferations of cells associated with primordial invaginating hair follicles, which were hyperchromatic but cytologically normal. At 18.5 dpc, the epidermal proliferations often involved most of the epidermal surface (Fig. 2, B and C). In mildly affected embryos, one or two epidermal growths were interspersed with six to eight follicles that appeared normal (Fig. 2D). In human BCCs, epidermal cells pro-

A. E. Oro, Howard Hughes Medical Institute, Departments of Dermatology, Developmental Biology, and Genetics, Stanford University School of Medicine, Stanford, CA 94305–5427, USA.
K. M. Higgins and M. P. Scott, Howard Hughes Medical Institute, Departments of Developmental Biology and Genetics, Stanford University School of Medicine, Stanford, CA 94305–5427, USA.
Z. Hu, J. M. Bonifas, E. H. Epstein Jr., Department of Dermatology, San Francisco General Hospital, University of California, San Francisco, CA 94110, USA.
*To whom correspondence should be addressed. E-mail addresses: scott@cmgm.stanford.edu, ehepstein@orca.ucsf.edu

liferate and form peripheral "palisades," a columnar epithelium resembling the basal keratinocyte layer. BCCs lack cell adhesion molecules that normally attach basal cells to the basement membrane zone, resulting in clefts between the basement membrane and tumor (*15*). These histological features of human BCCs were also found in the epidermal proliferations of K14-*Shh* transgenics (Fig. 2E).

The profile of marker proteins in the murine growths paralleled that of human BCCs. Human BCCs express basal keratins such as K14, do not express markers of differentiating stratified epithelium such as loricrin (*16*), and produce keratins associated with hyperproliferation, such as keratin 6, in the overlying epidermis (*16, 17*). Basement membrane proteins such as laminin 5 (Lam5) and bullous pemphigoid antigen 2 (BPAG2) are expressed at reduced levels in BCCs (*18*). In each of these respects, the K14-*Shh*–induced skin growths resembled BCCs. At 18.5 dpc, the growths were K14-positive (Fig. 3B) and did not express suprabasal differentiation markers (Fig. 3D). The interfollicular stratifying epithelium appeared to differentiate normally (Fig. 3, C and D), with hyperproliferation in overlying epidermis as revealed by keratin 6 expression (Fig. 3F). Both Lam5 (Fig. 3H) and BPAG2 (Fig. 3J) production was lower in K14-*Shh* proliferations than in control epidermis, as in BCCs (*18*). Excess SHH therefore has little effect on stratifying epidermis but causes growth of invaginating hair follicles into BCC-like tumors.

BCCs depend on the surrounding stroma for continued growth. Malignant tumors metastasize upon transplantation into mice, but transplanted BCCs undergo growth arrest or differentiation (*19*). Donor skin from 18.5-dpc K14-*Shh* transgenic embryos, marked with black or agouti hair, was transplanted to the dorsum of *scid* mice with white hair and examined 3, 5, and 10 weeks later (*20*) (Fig. 2, G to J). In each of 16 control grafts, the epithelium matured normally into wild-type hair follicles (Fig. 2G). In each of eight transgenic grafts, markedly reduced numbers of pigmented hairs were observed (Fig. 2H), showing that *Shh* can interfere with hair development. Transplanted transgenic skin growths did not enlarge and were partially differentiated. Epithelial growths in five grafts showed signs of mature hair follicle differentiation, including multiple mature hair shafts, sebaceous glands, and cysts in the invagination (Fig. 3, I and J). There was no evidence of metastasis. Thus, as with human BCCs, continued growth of tumors in the transgenics requires the proper tissue context.

The sufficiency of SHH for inducing tumors led us to search for human *Shh* mutations. A preliminary screen of human tumors revealed a *Shh* mutation in 1 of 43 BCCs, 1 of 14 medulloblastomas, and 1 of 6 breast carcinomas. These mutations were not detected in blood samples from the same patients (*21*) nor in blood DNA from 100 normal individuals (Fig. 4, A and B) (*22*). Remarkably, the three tumors contained the same mutation, a change of His^{133} to Tyr. Human His^{133}, equivalent to His^{134} in the mouse sequence, is located on the surface of SHH that may interact with a substrate for the hypothetical peptidase reaction (Fig. 4C) (*7*). The independent occurrence of the same mutation three times in tumors raises the possibility that human His^{133} to Tyr is a gain-of-function mutation of *Shh*. No biochemical assay is yet available for the putative zinc hydrolase activity, but in vivo tests may reveal altered activities of the changed signaling molecule.

Normally *Shh* is expressed in localized areas to control pattern formation. Ubiquitous epidermal expression would reduce or erase the asymmetry, preventing normal digit fates and interfering with formation of dorsal neural tube–derived structures

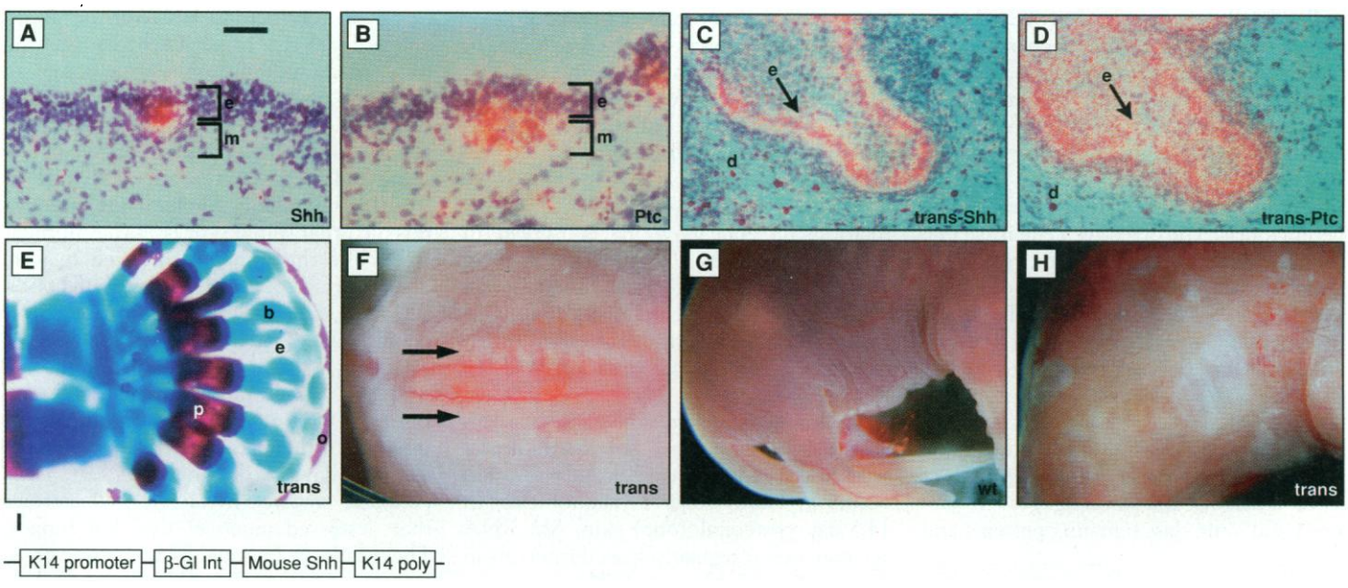

Fig. 1. Expression and phenotypes of normal and transgenic mouse skin. ^{35}S-labeled (red) antisense *Shh* and *ptc* probes were used to detect expression patterns by in situ hybridization (*32*). (**A**) Focal ectodermal (e) *Shh* RNA accumulation (red grains) in regularly spaced arrays in a presumptive follicle of 14.5-dpc trunk skin. (**B**) Accumulation of *ptc* in both the ectodermal cells (e) where *Shh* RNA is expressed and the underlying mesenchymal cells (m). (**C** and **D**) Sections of 18.5-dpc transgenic (trans) skin growths hybridized with (C) *Shh* or (D) *ptc* probes. The highest levels of *Shh* are in the transgenic epithelium (e), with *ptc* RNA accumulation in epithelial and neighboring dermal (d) cells. (**E** through **H**) Transgenic animals display marked skeletal and skin phenotypes. (E) Transgenic forepaw stained with alizarin red (calcified bone) and alcian blue (cartilage) provides an example of the polydactyly that is frequently observed. There are ectopic centers of cartilage between digits (e), terminal phalangeal bifurcations (b), and a persistent rim of ossification at the distal rim (o) (p, phalanx). (F) An 18.5-dpc transgenic embryo that failed to form dorsal spinal processes. This defect leads to a lack of closure of the spinal canal (arrows) and spina bifida. (G) Skin from a wild-type 18.5-dpc embryonic mouse showing regularly spaced skin folds. (H) Skin from a transgenic mouse showing translucent plaques and a lack of normal folds. (**I**) Schematic of the K14-*Shh* transgene, including the K14 promoter fragment, the β-globin 5′ intron, and the K14 polyadenylation sites (*12*). The bar in (A) represents 40 μm, for (A) through (D). Skeletal preparations were prepared as in (*33*).

(6, *23*). In BCNS patients, the haploinsufficiency of *ptc* may sensitize anterior limb or dorsal neural tube tissues to normal levels of *Shh*, resulting in polydactyly or spina bifida. That a twofold change in PTC dose may cause such changes in humans suggests that a precise balance between SHH and PTC is required.

The expression of *Shh* in basal keratinocytes is sufficient to induce mouse skin tumors that are indistinguishable from human BCCs. This effect of *Shh* may be completely unrelated to its normal function in skin development; *Shh* targets induced at high levels could create novel cell types and growth properties. However, the patterns of *Shh* and *ptc* transcription in the developing follicle are consistent with a normal role in controlling the proliferation of basal cells in the follicular epithelium. The decrease in mature hairs in the grafts along with the presence of abortive hair follicles in differentiating tumor buds suggests that SHH stimulates the growth of pluripotent follicular epithelium at the expense of differentiation. Such a role is supported by recent studies in chick feather bud development, where *Shh* induces feather bud outgrowth (*24*). Juxtaposition to a novel tissue environment appears to inhibit *Shh* activity, resulting in follicular differentiation.

The rapid and frequent appearance of *Shh*-induced tumors suggests that disruption of the SHH-PTC pathway is sufficient to create BCCs. The mouse BCCs appear within the first 4 days of skin development, unlike mouse squamous neoplasia, where tumors arise 1 to 12 months after oncogene expression (*25*). The K14-*Shh* tumor kinetics are consistent with previous clinical and epidemiologic data, which suggest that BCCs, in contrast to melanomas and squamous cell carcinomas, lack precursor or intermediate cellular phenotypes (*2*).

The gene *ptc* joins *APC* in a class of

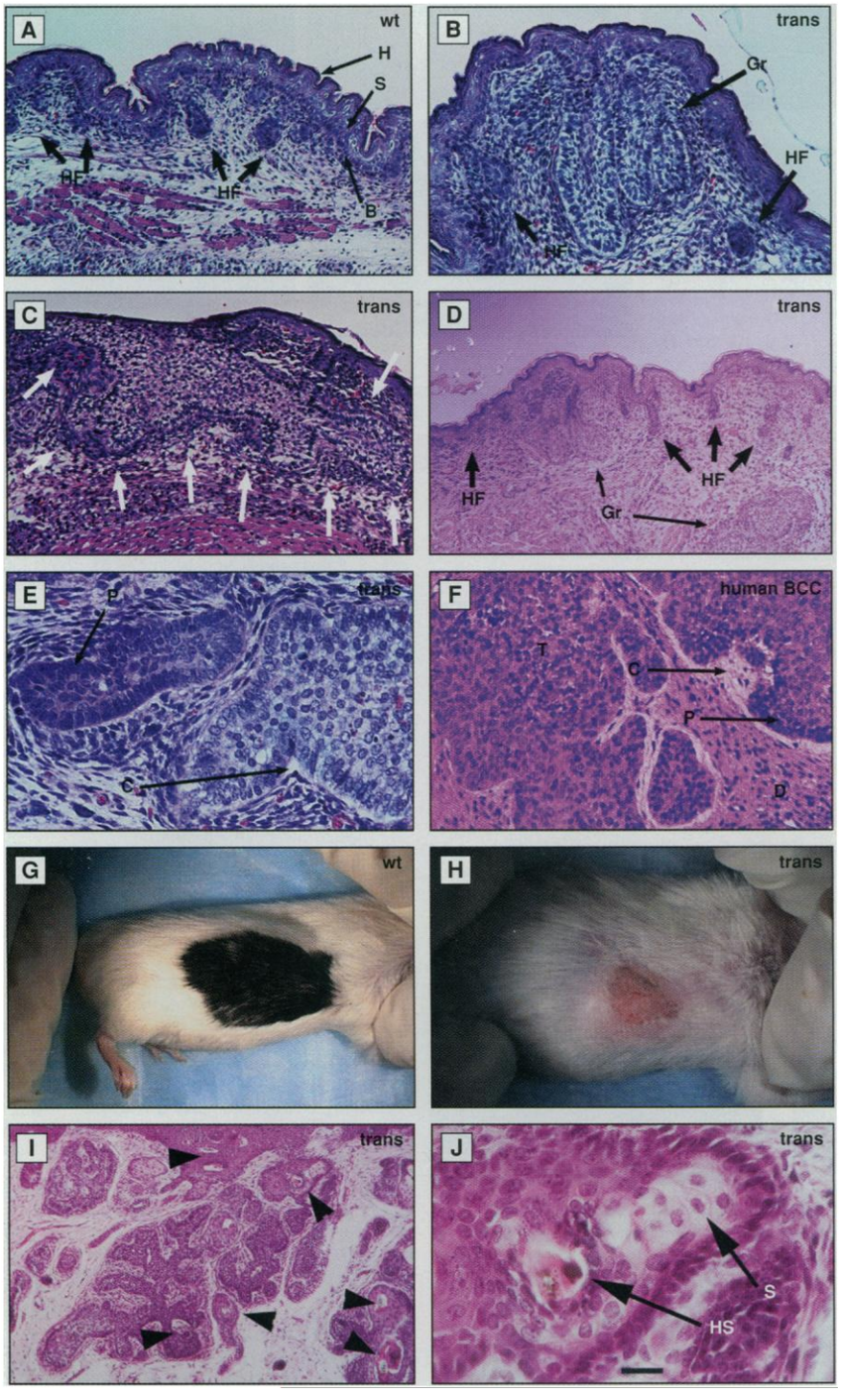

Fig. 2. (A through E) Skin histology of K14-*Shh* transgenic skin. Hematoxylin-eosin–stained sections of wild-type (wt) and transgenic (trans) mouse skin reveal a marked proliferation of the follicular epithelium. (**A**) Wild-type 17.5-dpc embryo showing normal keratinization and hair bud formation. Note spacing of hair follicles (HF) and wild-type basal (B), squamous (S), and horny (H) layers of stratifying epithelium. (**B**) Sagittal sections of transgenic 17.5-dpc trunk skin showing a massive downward growth (Gr) of an apparent hair follicle. Note the large size of the invagination compared to adjacent, apparently wild-type hair follicles (HF). (**C**) Marked proliferation of cells in a 17.5-day, strongly affected mutant embryo. Note the extensive epidermal growth pattern, which encompasses most of the basal cells (outlined by white arrows). (**D**) Lower power view of sections from mildly affected skin showing the regular number and spacing of many primary hair follicles (HF) with intermittent follicles forming downward growths (Gr). (**E**) High-power view of cells showing the artifactual clefting around proliferating cells (C), and peripheral palisading of columnar cells (P), characteristic of BCCs. (**F**) Paraffin-embedded section of human nodular BCC showing the above characteristics. T, tumor tissue; D, dermis. (**G** and **H**) Photographs of 5-week post-graft skin from B6CBF2 wild-type (G) and transgenic (H) skin grafted onto CB.17 *scid/scid* recipients (*20*). Note the dramatic reduction in pigmented hair in the graft. (**I**) Low- and (**J**) high-power view of haemotoxylin-eosin stain of paraffin-embedded skin showing the ongoing differentiation of BCCs into mature hair follicle epithelium. Note the lack of clefting and the presence of multiple mature hair shafts (arrowheads, HS) and sebaceous glands (S) in each tumor bud. Skin grafts performed as in (*27*). Bar in (J) represents 32 μm for (E) and (J), 80 μm for (A) through (C), (F), and (I), and 200 μm for (D).

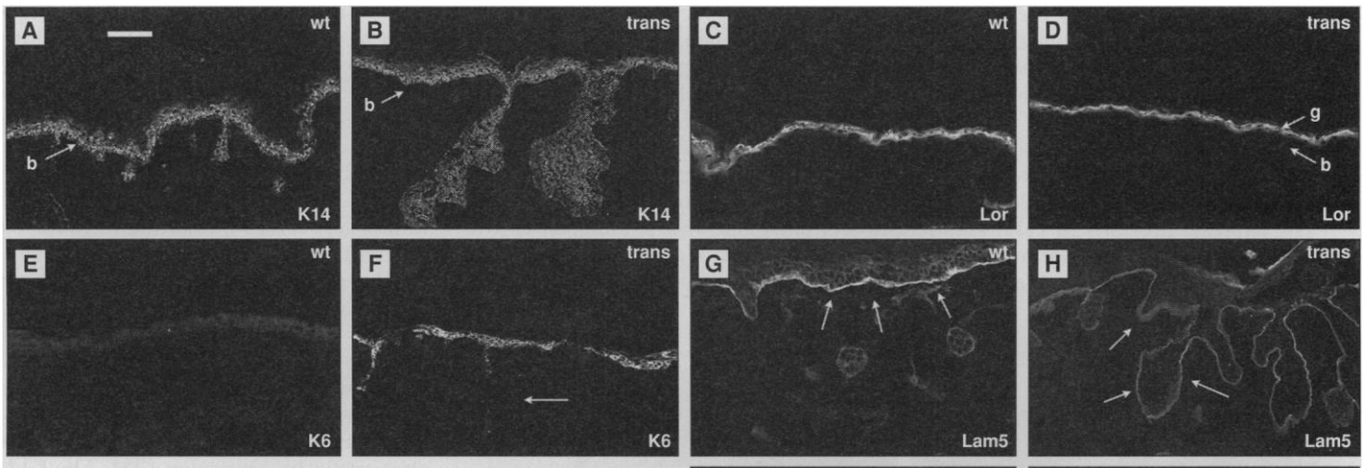

Fig. 3. Expression of BCC marker proteins in mouse tumors. Immunologic characterization of 18.5-dpc wild-type (wt) and transgenic (trans) skin. For a normal bright-field image, see Fig. 2A. (**A** and **B**) Staining of antibodies to K14 reveals that the epidermal proliferations express basal keratins. (**C** and **D**) Loricrin (Lor) shows normal granular staining (G), which is consistent with the normal differentiation pattern of stratified epithelium. (**E** and **F**) Expression of keratin 6 (K6) increases in transgenic skin, consistent with hyperproliferation of the epithelium. Note the lack of induced staining in the epidermal growths, consistent with previous studies on human BCCs. (**G** and **H**) Antibodies to LAM5 reveal decreased expression in transgenic epithelium. Note the reduction in expression throughout the epithelium (arrows). (**I** and **J**) Antibodies to BPAG2 reveal a marked decrease of BPAG2 expression in invaginating epithelium (arrows) compared to basal epithelium (arrowheads). Immunohistochemistry of skin was performed as in (*34*). Bar in (A) represents 62 μm for (A) through (H) and 25 μm for (I) and (J). Fixed sections were treated with rabbit primary antibodies, followed by anti-rabbit rhodamine-conjugated secondary antibodies, and were visualized with the use of a Bio-Rad confocal microscope. B, basal layer; G, granular layer.

genes instrumental for controlling early epithelial proliferation. Mutations in *APC* cause familial adenomatous polyposis, a condition that predisposes individuals to many benign polyps, akin to the hundreds of nodular BCCs that can occur in BCNS patients (*1*). Nodular BCCs are reminiscent of polyps in colonic epithelium, as both lack aneuploidy and are locally invasive (*1*, *2*). However, only the initial stages of skin and colon epithelial growth are similar, as colonic polyps progress to metastatic lesions at a substantially greater rate. This could be due in part to the different sets of genes regulated by *ptc* and *APC*.

Activating mutations of *Shh* (or another *Hh*) may be an alternative pathway for BCC formation in humans. The mutation of human His^{133} (mouse His^{134}) to Tyr is a candidate. It is distinct from loss-of-function mutations reported for individuals with holoprosencephaly (*26*). It lies adjacent in the catalytic site to His^{134} (mouse His^{135}), one of the conserved residues thought to be necessary for catalysis. Our data provide evidence that *Shh* may be a dominant oncogene in multiple human tumors, a mirror to the tumor suppresser activity of the opposing *ptc* gene. The mouse model of the disease may be useful in devising strategies for treating the human disease.

Fig. 4. Mutations of *Shh* in human tumor tissues. (**A**) Direct sequencing from PCR products reveals a mutation in the human *Shh* sequence at His^{133} (mouse His^{134}) in BCC tumor tissue but not in the blood of the same individual. The particular nucleotide changed was the same for each tumor type. (**B**) The mutation was confirmed by restriction fragment length polymorphism. The mutation in tumor tissue (T) eliminates an MscI site in *Shh* (arrow) present in blood (B) or normal (N) controls. (**C**) Molecular model of murine SHH (*7*) reveals the position of mouse His^{134} (white atoms; equivalent to human His^{133}). Putative catalytic (green) and zinc coordinating (red) residues are located near the changed residue. Molecular modeling was performed with RasMac. M, marker; MED, medulloblastoma; Breast, breast carcinoma.

REFERENCES AND NOTES

1. E. Fearon and B. Vogelstein, *Cell* **61**, 759 (1990); K. Kinzler and B. Vogelstein, *ibid.* **87**, 159 (1996).
2. B. Barlogie *et al.*, *Cancer Res.* **43**, 3982 (1983); R. Marks, G. Rennie, T. Selwood, *Arch. Dermatol.* **124**, 1039 (1988); S. J. Miller, *J. Am. Acad. Dermatol.* **24**, 161 (1991); D. Miller and M. Weinstock, *ibid.* **30**, 774 (1994).
3. R. Gorlin, *Dermatol. Clin.* **13**, 113 (1995).
4. H. Hahn *et al.*, *Cell* **85**, 841 (1996); R. L. Johnson *et al.*, *Science* **272**, 1668 (1996); A. Unden *et al.*, *Cancer Res.* **56**, 4562 (1996); A. Chidambaram *et al.*, *ibid.*, p. 4599.
5. A. G. Quinn, C. Campbell, E. Healy, J. L. Rees, *J. Invest. Dermatol.* **102**, 300 (1994); M. Gailani *et al.*, *Nature Genet.* **14**, 78 (1996).
6. P. W. Ingham, *Curr. Opin. Genet. Dev.* **5**, 492 (1995); M. Dean, *Nature Genet.* **14**, 245 (1996); N. Perrimon, *Cell* **86**, 513 (1996); M. Hammerschmidt, A. Brook, A. P. McMahon, *Trends Genet.* **13**, 14 (1997).
7. T. Hall, J. Porter, P. Beachy, D. Leahy, *Nature* **378**, 212 (1996).
8. P. Ingham, *ibid.* **366**, 560 (1993).
9. M. J. Bitgood and A. P. McMahon, *Dev. Biol.* **172**, 126 (1995); S. Iseki *et al.*, *Biochem. Biophys. Res. Commun.* **218**, 688 (1996).
10. The accumulation of *Shh* RNA is seen ectodermally later in development and in the anagen hair matrix, with *ptc* RNA accumulating in adjacent cells.
11. The Eco RI–Spe I fragment of the mouse *Shh* cDNA, which includes the entire cDNA and the first 400 base pairs (bp) of the 3′ untranslated region, was placed into the keratin β-globin promoter cassette (*12*). The cassette was microinjected into the pronucleus of B6CBF2 zygotes, and transgenic embryos were identified by standard techniques.
12. C. Byrne and E. Fuchs, *Development* **120**, 2369 (1994); M. Saitou *et al.*, *Nature* **374**, 159 (1995).
13. J. C. Izpisua-Belmonte, D. A. Ede, C. Tickle, D. Duboule, *Development* **114**, 959 (1992); P. H. Francis-West *et al.*, *Dev. Dyn.* **203**, 187 (1995).
14. Rib abnormalities, such as abnormal fusion at the

sternum, and lower jaw aplasia were also commonly seen.
15. W. F. Lever and G. S. Lever, *Histopathology of the Skin* (Lippincott, Philadelphia, 1990); S. Miller, *J. Am. Acad. Dermatol.* **24**, 1 (1991).
16. A. C. Markey, E. B. Lane, D. M. MacDonald, I. M. Leigh, *Br. J. Dermatol.* **126**, 154 (1992).
17. A. Stoler, R. Kopan, M. Duvic, E. Fuchs, *J. Cell. Biol.* **107**, 427 (1988).
18. J. Stanley, J. Beckwith, R. Fuller, S. Katz, *Cancer* **50**, 1486 (1982); P. Savoia, L. Trusolino, E. Pepino, O. Cremona, P. Marchisio, *J. Invest. Dermatol.* **101**, 352 (1993); Z. Lazarova, N. Domloge-Hultsch, K. Yancey, *Exp. Dermatol.* **4**, 121 (1995); J. Fairley, P. Heintz, M. Neuburg, L. Diaz, G. Giudice, *Br. J. Dermatol.* **133**, 385 (1995).
19. M. Cooper and H. Pinkus, *Cancer Res.* **37**, 2544 (1977); R. E. Grimwood *et al.*, *Cancer* **56**, 519 (1985); G. Stamp, A. Quaba, A. Braithwaite, N. A. Wright, *J. Pathol.* **156**, 213 (1988); S. Hales, G. Stamp, M. Evans, K. Fleming, *Br. J. Dermatol.* **120**, 351 (1989).
20. We performed mouse skin grafts as in (*27*), except that we used transgenic or wild-type dorsal trunk skin from B6CBF2 embryos that had been dissected away from underlying muscle and grafted it onto 8- to 12-week-old male *scid* recipient mice. Dressings were removed after 3 weeks. Each animal was photographed weekly.
21. Genomic sequences containing *SHH* were isolated from a bacterial artificial chromosome library obtained from Research Genetics. Primers used to screen this library from exon 2 [ACC GAG GGC TGG GAC GAA GAT GGC and GCG AGC CAG CAT GCC GTA CTT GCT G (*28*)] identified BAC 270A17, which was digested with restriction enzymes and ligated with vectorette linkers (*29*). Exon-intron boundaries for the three exons were determined by sequencing polymerase chain reaction (PCR) products amplified using the universal vectorette primer and *SHH* cDNA primers selected from published sequences. Since we were unable to obtain sequences from the exon 2–intron 3′ boundary, a primer from the 3′ end of exon 2 was used. Primers used to amplify genomic SHH were as follows: exon 1, CCG CCG CGC GCA CTC G and AAG GAG CGG GTG AAA TCA CC; exon 2, TAA CGT GTC CGT CGG TGG G and TGC TTT CAC CGA GCA GTG G; and exon 3, CCT CCT CCC CGA GAC GC and GGC CCC CTC CCG CGC C. Mutations were identified by single-strand conformation polymorphism (SSCP) analysis of PCR products amplified from genomic DNA. The PCR products were sequenced on both strands directly from the PCR-produced templates and after cloning into Bluescript. Subsequent to our completion of this work, another group has published intron sequences and primers useful for amplifying SHH exons from genomic DNA (*26*).
22. DNA from one other BCC had a methionine to isoleucine change at position 115, but this change was also present in DNA from the patient's blood. This unusually large BCC was diagnosed at age 40 in a patient with no other phenotypic abnormalities suggestive of BCNS.
23. K. F. Liem, G. Tremmi, H. Roelink, T. M. Jessell, *Cell* **82**, 969 (1995); H. Roelink *et al.*, *ibid.* **81**, 445 (1995); C. Tabin, *ibid.* **80**, 671 (1995); M. J. Cohn and C. Tickle, *Trends Genet.* **12**, 253 (1996).
24. S. Ting-Berreth and C. Chuong, *Dev. Dyn.* **207**, 157 (1996).
25. J. Arbeit, *Cancer Surv.* **26**, 7 (1996).
26. E. Belloni *et al.*, *Nature Genet.* **14**, 353 (1996); E. Roessler *et al.*, *ibid.*, p. 357.
27. D. Medalie, *J. Invest. Dermatol.* **107**, 121 (1996).
28. V. Marigo *et al.*, *Genomics* **28**, 44 (1995).
29. J. Riley *et al.*, *Nucleic Acid Res.* **18**, 2887 (1990).
30. Y. Echelard *et al.*, *Cell* **75**, 1417 (1993).
31. L. Goodrich, R. Johnson, L. Milenkovic, J. A. McMahon, M. Scott, *Genes Dev.* **10**, 301 (1996).
32. In situ hybridization studies were performed on mouse embryonic skin with the use of antisense and sense control probes and standard techniques. The *Shh* template (*30*) was a mouse *Shh* partial cDNA missing 300 bp of the 3′ coding region. The *ptc* template was M2-3, an 841-bp cDNA fragment from the 5′ end of the coding region (*31*).
33. T. Lufkin *et al.*, *Nature* **359**, 835 (1992).
34. L. Guo, Q.-C. Yu, E. Fuchs, *EMBO J.* **12**, 973 (1993).
35. We thank H. Fan and P. Khavari for instruction in skin grafting techniques and the Scott lab, D. Kingsley, A. McMahon, E. Fuchs, B. Smoller, A. Rothman, J. Xie, and C. Tabin for clones and advice. We thank D. Roop (K14), Z. Liu (BPAG2), J. P. Ortonne (Lam5), and S. Yuspa (K6) for antibodies. A.E.O. was supported by a grant from the National Institute for Arthritis and Musculoskeletal Diseases. Research in San Francisco was supported by NIH grant AR39959. M.P.S. is an Investigator of the Howard Hughes Medical Institute and this research was done with the Institute's support. Human and mouse work was done according to NIH Human Subjects and Animal Use Guidelines at each institution.

22 January 1997; accepted 3 March 1997

Integration of What and Where in the Primate Prefrontal Cortex

S. Chenchal Rao, Gregor Rainer, Earl K. Miller*

The visual system separates processing of an object's form and color ("what") from its spatial location ("where"). In order to direct action to objects, the identity and location of those objects must somehow be integrated. To examine whether this process occurs within the prefrontal (PF) cortex, the activity of 195 PF neurons was recorded during a task that engaged both what and where working memory. Some neurons showed either object-tuned (what) or location-tuned (where) delay activity. However, over half (52 percent, or 64/123) of the PF neurons with delay activity showed both what and where tuning. These neurons may contribute to the linking of object information with the spatial information needed to guide behavior.

Anatomical segregation of processing is an important principle of neural organization. Even within a modality, largely separate pathways process different attributes of the same stimulus. Perhaps the best explored example of segregation is in the visual system, where the analysis of visual scenes is carried out by at least two pathways. A "ventral pathway" through inferior temporal (IT) cortex processes information about features that identify objects, such as shape and color (object, or "what" information), and a "dorsal pathway" through posterior parietal (PP) cortex processes information about location and spatial relations among objects (spatial, or "where" information) (*1*). This example raises the question of where and how information about object identity is integrated with information about object location. One region that may play a role in integration is the prefrontal (PF) cortex, which receives inputs from virtually all of the brain's sensory systems (*2*) and has long been thought to be an area where diverse signals are integrated to serve higher order cognitive functions.

A major contribution of the PF cortex to cognition is the active maintenance of behaviorally relevant information "online," a process known as working memory (*3*). Working memory is typically studied in tasks in which an animal must remember a cue stimulus over a delay period and then make a behavioral response based on the cue. Physiological studies in monkeys have revealed that many PF neurons are highly active during the delay of such tasks (*4*). The activity is often cue-specific, suggesting that this "delay activity" is the neural correlate of the working memory trace. Given its central role in cognition, PF neurons that contribute to working memory are obvious candidates for integrating diverse signals. However, the extent to which different types of information, such as what and where, are integrated within the PF cortex is not well understood. Highly processed spatial information from the PP cortex and object information from the IT cortex are received by separate regions of the PF cortex, the dorsolateral (areas 46 and 9) and the ventrolateral (area 12) PF cortex, respectively (*5*), but there are interconnections between these regions that could bring what and where together (*2*, *6*).

Physiological studies have found that different neurons and even different regions of the PF cortex convey either object information (in the ventrolateral PF cortex) or spatial information (in the dorsolateral PF cortex), but no neurons have been reported to convey both (*7*). In previous studies, however, working memory for what and where was examined in two separate tasks: an object task and a spatial task. This separation rarely occurs in the real world and it raises the possibility that the apparent segregation of what and where working memory reflected an artificial behavioral segregation. Thus, to investigate whether object and spatial information is integrated by in-

Department of Brain and Cognitive Sciences and The Center for Learning and Memory, Massachusetts Institute of Technology, Cambridge, MA 02139, USA.

*To whom correspondence should be addressed. E-mail: ekm@ai.mit.edu